LANGMUIR

pubs.acs.org/Langmuir Article

Understanding Separation of Oil–Water Emulsions by High Surface Area Polymer Gels Using Experimental and Simulation Techniques

Pratik S. Gotad,[§] Abdol Hadi Mokarizadeh,[§] Mesfin Tsige,* and Sadhan C. Jana*

Cite This: *Langmuir* 2024, 40, 24622–24633 Read Online

ACCESS | Metrics & More | Article Recommendations | Supporting Information

ABSTRACT: This work examines the functional dependence of the efficiency of separation of oil–water emulsions on surfactant adsorption abilities of high surface area polymer gels. The work also develops an understanding of the factors and steps that are involved in emulsion separation processes using polymer gels. The work considers four polymer gels offering different surface energy values, namely, syndiotactic polystyrene (sPS), polyimide (PI), polyurea (PUA), and silica. The data reveal that surfactant adsorption abilities directly control the emulsion separation performance. The gels of sPS and PI destabilize the emulsions due to significant surfactant adsorption. The surfactant-lean oil droplets are then absorbed in the pores of sPS and PI gels due to the preferential wettability of the oil phase. The PUA and silica gels are more hydrophilic and show a lower surfactant adsorption ability. These gels cannot effectively remove the surfactant molecules from the emulsions, leading to a poor emulsion separation performance. The study uses simulation data to understand the adsorption characteristics of two poly(ethylene oxide)-poly(propylene oxide)-poly(ethylene oxide) block copolymer surfactants. The simulation results are used for the interpretation of emulsion separation performance by the gels.

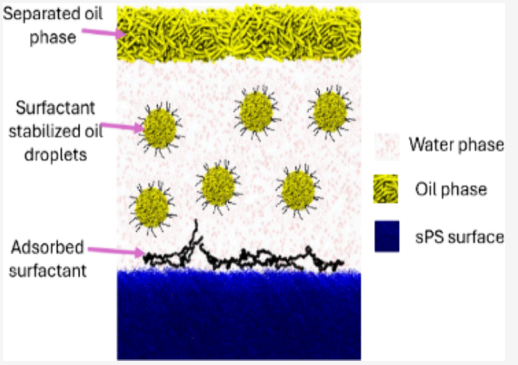

1. INTRODUCTION

Oil-in-water or water-in-oil emulsions are frequently encountered in crude oil production, enhanced oil recovery processes, oily industrial effluents, or recurrent oil spills.[1,2] The presence of highly viscoelastic surfactant films at the oil–water interfaces stabilizes the emulsions, which in turn causes severe problems of fouling and corrosion of process equipment and leads to higher production and operating costs.[3] Several techniques have been developed over the years to break the emulsions, such as use of chemical additives,[4] thermal treatment[5] or microwave irradiation,[6,7] membrane separation,[8] and electric[9] or acoustic fields.[10] These techniques suffer from several shortcomings, such as secondary pollution, low separation efficiencies, and high cost in terms of capital and energy consumption.[11,12] To alleviate some of the above concerns, high surface area polymer gels were considered in recent work for oil–water emulsion separation.[13,14] The polymer gels function well due to their ability to remove the surfactants from liquid–liquid interfaces via adsorption. Conventional oil–water emulsion separation materials work on the principle of either size exclusion of the droplets or change of the surface wettability of the filter media to allow only one liquid phase to pass through it. The polymer gels used in this work exploit the cooperative functioning of surfactant adsorption on polymer strand surfaces and oil absorption inside the pores of the gels to achieve emulsion separation.

Surfactant molecules readily go to oil–water interfaces due to their amphiphilic nature, thus lowering the interfacial tension between water and oil. The steric or electrostatic barriers imposed by the surfactant molecules at oil–water interfaces inhibit droplet coalescence that is otherwise promoted by the attractive van der Waals forces.[3,15] In an unstable emulsion, the dispersed phase droplets flocculate, coalesce, and eventually segregate into a separate bulk liquid phase.[16] An effective emulsion destabilizer can deplete the surfactant molecules from the continuous liquid phase and from the oil–water interfaces. In this regard, chemical demulsification is the most common. Chemical demulsifiers work by penetrating or rupturing the existing surfactant films.[3,17,18] The new film formed by the demulsifier is weaker in strength and thus facilitates the coalescence of the oil droplets. A few examples of chemical demulsifiers are cationic quaternary ammonium salts,[19,20] acrylic latex-based polymers, dendrimers,[21] ionic liquids,[22,23] and graphene oxide nanosheets.[18] However, the use of chemical demulsifiers does not provide a permanent solution as mixing or agitation inherent to the process can lead to emulsification by the surfactants still

Received: September 5, 2024
Revised: October 15, 2024
Accepted: October 28, 2024
Published: November 8, 2024

https://doi.org/10.1021/acs.langmuir.4c03496
Langmuir 2024, 40, 24622–24633

present in the system. The chemical demulsifiers added to the liquid stream may serve as a source of secondary pollution.

Katepalli et al. alleviated the concerns of chemical demulsifiers by introducing colloidal fumed silica particles as demulsifiers for a nonionic Triton X100 stabilized oil-in-water emulsion.[16] The partially hydrophobic silica particles remove the surfactant via adsorption by H-bonding and hydrophobic interactions, which lead to flocculation and coalescence of oil droplets. However, fumed silica is considered a pollutant, and the removal of remnant, extremely small silica particles, from the liquid streams is a challenge. In the above context, our research investigated a new demulsification pathway that uses high surface area polymeric gels for adsorption of large amounts of surfactant molecules from liquids.[24] The polymer gels can be easily removed from the system, and the process does not contaminate the liquids with particulate matter or small-molecule chemical agents.

Polymer gels formed by both chemical and physical cross-linking processes[25−27] provide an extremely high specific surface area (200−900 m^2/g) with interconnected pore networks consisting of mesopores (2−50 nm) and macropores (>50 nm). Syndiotactic polystyrene (sPS),[27−29] polyimide (PI),[30,31] polyurea (PUA),[24,32,33] cellulose,[31,32] silica,[35] and polyurethane[36] are examples of gel-forming polymer systems. We recently investigated the adsorption performance of nonionic surfactants based on a poly(ethylene oxide) (PEO)-poly(propylene oxide) (PPO)-poly(ethylene oxide) (PEO) block copolymer by several polymer gels differing in surface energy values.[24] The study reported significant surfactant adsorption by the sPS gels attributed to the high interfacial energy and high specific surface area of the polymer gels. A much stronger adsorption was observed when the surfactant concentration was greater than the critical micelle concentration (CMC). The work[24] becomes immediately relevant for oil−water separation as the polymer gels can effectively remove the surfactants at or above the CMC values. A typical surfactant-adsorbing material shows a plateau in surfactant adsorption capacity as the surfactant concentration approaches the CMC value.[37−39] In this context, many surfactant-adsorbing materials are not appropriate for demulsification. The earlier study[24] and the present work on high specific surface area, high porosity meso-macroporous polymer gels present interesting alternatives.

The present work evaluated the effects of surface energy of polymer gels on adsorption of nonionic PEO-PPO-PEO block copolymer surfactants and their influence on the stability of oil-in-water emulsions. Besides, polymer gels with a high porosity and small capillary pores can absorb the oil phase. Therefore, the emulsion separation process can have contributions from both surfactant adsorption onto the polymer gel surface and oil absorption by the pores present in the polymer gels. The above roles of polymer gels were evaluated in this work by considering two nonionic PEO-PPO-PEO block copolymer surfactants, one with short chains and the other with long chains. An atomistic simulation technique was used in conjunction to clearly delineate the adsorption of short- and long-chain PEO-PPO-PEO surfactants onto polymer surfaces. The preferential adsorption of short-chain surfactants on the polymer gel surface was analyzed in terms of structural configuration, binding energy, and the surface area occupied by the molecules. The implications of these results on the oil−water emulsion separation are discussed in this paper.

2. EXPERIMENTAL SECTION

2.1. Materials. sPS (Mw ≈ 300 000 g/mol, 98%) was obtained from Scientific Polymer Producers Inc. (Ontario, NY, USA). The diamine, 2,2′dimethylbenzidine (DMBZ), was purchased from Shanghai Worldyang Chemical Co., Ltd. (Shanghai, China). Pyromellitic dianhydride (PMDA, purity ≥ 96.5%), tris(2-aminoethyl) amine (TREN, purity ≥ 95.5%) cross-linker, acetic anhydride (≥99%), and toluene (≥99.9%) were purchased from Sigma-Aldrich (Milwaukee, WI, USA). Pyridine (≥99%) and acetone (≥99.5%) were purchased from Fisher Scientific (Ontario, NY, USA). *N*,*N*-Dimethylformamide (DMF, ≥99.5%) was purchased from VWR International (Radnor, PA, USA). Ethanol was purchased from Decon Laboratories Inc. (King of Prussia, PA, USA). Desmodur N3300A (tri-isocyanate) and triethylamine (TEA) were procured from Covestro (Pittsburgh, PA, USA) and Sigma-Aldrich (Milwaukee, WI, USA), respectively. Pluronic L35 (PL35) and Pluronic F127 (PF127) each with a molecular weight of 1900 and 12,600 g/mol, respectively, along with sodium dodecyl sulfate (SDS) and cetyltrimethylammonium bromide (CTAB) were obtained from Sigma-Aldrich (Milwaukee, WI, USA). Tetraethyl orthosilicate (TEOS, reagent grade, 98%), nitric acid (purity, 64−66%), and ammonium hydroxide solution (28−30%) were purchased from Sigma-Aldrich (Milwaukee, WI, USA). Ultralow sulfur diesel (ULSD) fuel was procured from a local gas station and was treated with a Fuller's Earth Filter (Jaxon Filtration, GA) to remove the impurities and surfactants, if any. All of the chemicals were used as received.

2.2. Fabrication of sPS Gels and Aerogels. sPS gels were prepared using the thermoreversible gelation mechanism of sPS solutions in toluene. sPS pellets were dissolved in toluene in sealed vials at 100 °C to produce a solid concentration of 0.06 g/mL. The solution was allowed to cool under ambient conditions for 1 min and was subsequently poured in cylindrical glass molds of diameter 15 mm for gelation. The gels were allowed to age in the mold for 5 h to ensure complete gelation and were then demolded and solvent-exchanged first with ethanol and finally with deionized water to obtain the water-filled sPS gels. To form the diesel-filled sPS gels, the ethanol-filled sPS gels were exchanged with acetone followed by solvent exchange with diesel.

The sPS aerogels were obtained by solvent exchanging ethanol-filled gels with liquid carbon dioxide followed by supercritical drying at 50 °C and 11 MPa. The sPS aerogels were used for the determination of surface energy, pore sizes, and internal structural morphology.

2.3. Fabrication of Polyimide Gels and Aerogels. PMDA and DMBZ were mixed for 2 min at room temperature and 1200 rpm magnetic stir bar angular speed followed by addition of TREN, acetic anhydride, and pyridine. The resulting solution was poured into a cylindrical mold of diameter 16 mm and allowed to gel for 10 min. The gels were then allowed to age for 24 h and removed from the mold. The gels were subsequently solvent-exchanged with DMF−acetone mixtures with 75:25, 50:50, and 25:75 v/v followed by three additional solvent exchange steps with 100% acetone. The water-filled polyimide gels were obtained by solvent exchanging with acetone−DI water mixtures of increasing water concentrations and finally with 100% DI water. Similarly, the diesel-filled polyimide gels were obtained by solvent exchanging acetone-filled gels with 100% diesel six times. Polyimide gels with 7.5 wt % polymer concentration were prepared using 0.686 g of PMDA, 0.636 g of DMBZ, 92 μL of TREN, 1.847 mL of acetic anhydride, and 1.909 mL of pyridine in 15 mL of DMF.

The acetone-filled polyimide gels were exchanged with liquid carbon dioxide and dried under supercritical carbon dioxide at 50 °C and 11 MPa pressure to obtain polyimide aerogels for morphology, wettability, and pore size characterization.

2.4. Fabrication of Polyurea Gels and Aerogels. The PUA gels were prepared using tri-isocyanate, water, and TEA in a molar ratio 1:3:1 with 0.15 M concentration of tri-isocyanate. The tri-isocyanate was dissolved in anhydrous DMF at room temperature for 30−45 min, deionized water was added, and it was mixed for 3 min.

https://doi.org/10.1021/acs.langmuir.4c03496
Langmuir 2024, 40, 24622−24633

TEA was added to the mixture, and it was mixed for an additional 2 min. The PUA gels filled with acetone were obtained by solvent exchange steps with mixed solvents DMF−acetone in ratios of 75:25, 50:50, and 25:75 v/v followed by three solvent exchanges in 100% acetone. The acetone-filled gels were solvent-exchanged in liquid CO_2 and subsequently dried under supercritical conditions of CO_2 at 50 °C and 11 MPa pressure to obtain aerogel specimens. Water-filled polyurea gels were prepared by solvent exchange with acetone−water mixtures with increasing concentrations of water and finally with 100% DI water three times. Diesel-filled polyurea gels were obtained by solvent exchanging acetone-filled gels with 100% diesel six times. Polyurea aerogels for characterization purposes were obtained by solvent exchanging acetone-filled gels in liquid CO_2 and subsequent drying under supercritical conditions of CO_2 at 50 °C and 11 MPa pressure.

2.5. Fabrication of Silica Gels and Aerogels. The silica gels were prepared by using tetraethyl orthosilicate (TEOS) (10.4 g) as the precursor monomer. TEOS was dissolved in an ethanol (10 mL) and water (2.6 mL) mixture. Nitric acid was added to it to partially hydrolyze TEOS at a pH of ∼2.0 and mixed for 10 min. Subsequently, a solution of ammonium hydroxide (NH_4OH) (0.25 mL), water (3.6 mL), and ethanol (20 mL) was added to it. The resulting solution was allowed to mix for 10 min and then was poured in cylindrical molds of diameter 1.5 cm. The sol was allowed to gel in the molds overnight. The gels were removed from the mold and solvent-exchanged with ethanol−water mixtures of 75:25, 50:50, and 25:75 v/v followed by four additional solvent exchange steps with 100% water to form the water-filled silica gels.

To obtain silica aerogels, the gels were solvent-exchanged with 100% ethanol six times followed by solvent exchanges with liquid carbon dioxide and supercritical drying in CO_2 at 50 °C and 11 MPa pressure.

2.6. Preparation of Surfactant-Stabilized Oil−Water Emulsions. The oil-in-water emulsions were obtained using water as the continuous phase and ultralow sulfur diesel (ULSD) fuel as the dispersed phase. Emulsions with 1 vol % ULSD in water were prepared using a planetary centrifugal THINKY mixer at 1000 rpm for 10 min. The surfactants, short-chain PL35 and long-chain PF127, at a concentration of 2 wt % (both above the CMC) were added to stabilize the emulsion. The emulsions were stable for the duration of experiments as inferred from the stable droplet size distributions examined via an optical microscope over a period of 24 h.

2.7. Simulation Details. The initial structures of Pluronic L35 and F127 were constructed using the Materials Studio package (Materials Studio, by Dassault Systèmes BIOVIA, UK (Accelrys), (License purchased by The University of Akron). Subsequently, single chains of PL35 and PF127 were immersed in 15,000 and 20,000 water molecules, respectively, utilizing the POLYMATIC package.[40] Molecular dynamics simulations were conducted using the LAMMPS package[41] applying periodic boundary conditions in all dimensions. The SPC/E[42] water model and the force field developed by Abbott et al.[43] for Pluronic molecules were utilized to characterize both bonded and nonbonded interactions, with a cutoff distance of 12 Å for van der Waals and short-range electrostatic interactions. Long-range electrostatic interactions were calculated using the PPPM algorithm[44] with an accuracy of 10^{-4}. The SHAKE algorithm was employed to fix the water bond length and angle.[45] The initial simulation box underwent equilibration for 15 ns under the NPT ensemble, with the temperature and pressure set to 298 K and 1 bar, respectively, using a Nose−Hoover thermostat and barostat. Once the box density reached equilibrium, simulations continued under the NVT ensemble at the same temperature. In all the simulations, the step time and dumping frequency were 1 fs and 5 ps, respectively, and the Verlet algorithm was used to solve time-dependent Newtonian equations of motion. The bulk simulation for PF127, featuring a greater number of monomers and slower dynamics, lasted over 480 ns, while PL35 required a shorter simulation time of 250 ns.

To integrate the polystyrene film into the water/polymer simulation box, periodicity in the *z*-direction of the equilibrated water/polymer box was eliminated. Subsequently, the new water−polymer box was positioned 3 Å above the polystyrene film. The syndiotactic polystyrene film consisted of 160 chains, each comprising 40 monomers. Its equilibrated dimensions were approximately 108 Å × 102 Å × 106 Å in the *x*, *y*, and *z* directions, containing a total of 103,200 atoms. Details regarding the preparation of the polystyrene film can be found elsewhere.[46] Furthermore, the OPLS-AA force field[47] was used to describe both bonded and nonbonded interactions of the polystyrene chains.

2.8. Characterization. *2.8.1. Bulk Density, Skeletal Density, and Porosity Measurements.* A helium pycnometer (AccuPyc II 1340, Micromeritics Instrument Corp., Norcross, GA) was used to measure the skeletal density (ρ_s) of the aerogel specimens, and the bulk density (ρ_b) was obtained by measuring their mass and volume. The porosity of aerogels was calculated using eq 1:

$$\rho_T = (1 - \rho_b/\rho_s)\times 100 \tag{1}$$

2.8.2. Brunauer−Emmett−Teller (BET) Adsorption−Desorption. N_2 adsorption−desorption isotherms obtained at 77 K using a Micromeritics Tristar II 3020 analyzer (Micromeritics Instrument Corp., Norcross, GA) were used to obtain the BET surface area and mesopore volume fraction of the aerogel samples. The mesopore volume was obtained using the nonlocal density functional theory model from N_2 isotherms at 77 K. The total pore volume (V_{total}), the mesopore volume fraction (ϕ_{meso}), and the macropore volume fraction (ϕ_{macro}) were obtained using eqs 2−4:

$$V_{total} = \frac{1}{\rho_b} - \frac{1}{\rho_s} \tag{2}$$

$$\phi_{meso} = \frac{V_{meso}}{V_{total}} \tag{3}$$

$$\phi_{macro} = \frac{V_{macro}}{V_{total}} = 1 - \phi_{meso} \tag{4}$$

In eqs 3 and 4, V_{meso} and V_{macro} are the total volumes of meso- and macropores, respectively.

2.8.3. Morphology. Scanning electron microscopy (SEM JSM 5310, JEOL, MA) was used to obtain the morphology of aerogel specimens.

2.8.4. Polymer Surface Energy and Contact Angle Measurements. The polymer surface energy was obtained as in eq 5.[46] The contact angle values of water and diiodomethane were measured on compressed polymer disks.

$$\gamma_{LS} = \gamma_L + \gamma_S - \frac{4\gamma_L^d\gamma_S^d}{\gamma_L^d + \gamma_S^d} - \frac{4\gamma_L^p\gamma_S^p}{\gamma_L^p + \gamma_S^p} \tag{5}$$

In eq 5, γ_{LS} is the interfacial tension between liquid and solid, γ_L is the surface tension of the liquid, γ_S is the surface energy of the solid, and γ_S^d and γ_S^p are the dispersion (nonpolar) and polar components of liquid surface tension, respectively. The standard values of γ_L^d = 21.8 dyn/cm and γ_L^p = 50.7 dyn/cm for water and γ_L^d = 44.1 dyn/cm and γ_L^p = 6.7 dyn/cm for diiodomethane were used in the calculations.[48] The surface energy of the polymer is obtained from the sum of dispersive (γ_S^d) and polar (γ_S^p) components as in eq 6:

$$\text{polymer surface energy}(\gamma_S) = \gamma_s^d + \gamma_s^p \tag{6}$$

The polymer−liquid interfacial energy (γ_{LS}) was calculated using the Young−Laplace equation as in eq 7, where γ_L is the surface tension of the liquid and θ is the contact angle on the polymer surface:

$$\gamma_S = \gamma_{LS} + \gamma_L \cos\theta \tag{7}$$

The polymer−water and polymer−diesel contact angles were obtained by placing a 10 μL droplet of the respective liquid on a compressed polymer disk. For this purpose, aerogel specimens were compressed as disks between two clean, flat metal plates at 1.8 MPa

https://doi.org/10.1021/acs.langmuir.4c03496
Langmuir 2024, 40, 24622−24633

Table 1. Surface Energy of sPS, PI, PUA, and Silica Gels along with Their Interfacial Energy

material	water contact angle (deg)	diiodomethane contact angle (deg)	polar component (mN/m)	dispersive component (mN/m)	polymer surface energy (mN/m)	interfacial energy (mN/m)
sPS	96 ± 1	41 ± 2	2.3	38.5	40.8	48.3
PI	77 ± 2	32 ± 3	10.6	34.4	45.1	28.7
PUA	64 ± 2	48 ± 1	19.9	25.5	45.5	13.7
silica	25 ± 3	27 ± 1	38	31	69	3.3

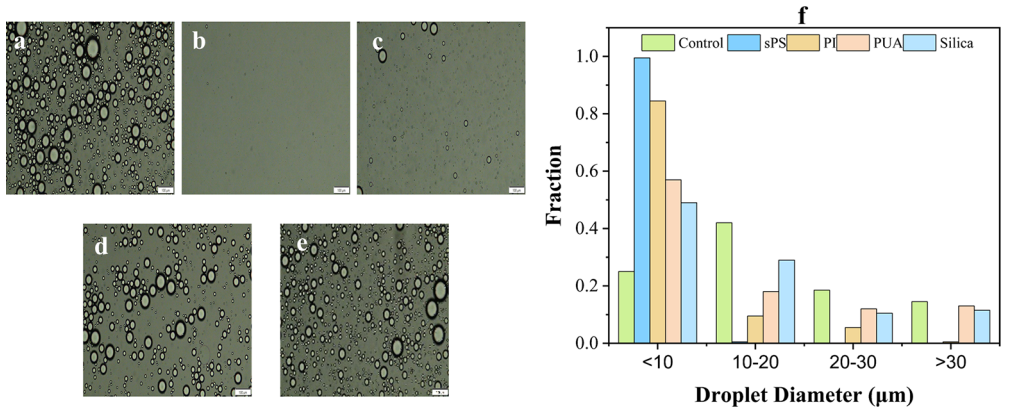

Figure 1. Optical microscopy images of oil-in-water emulsions. (a) Control emulsion and emulsions after they were bought in contact with (b)sPS, (c) PI, (d) PUA, (e) silica gels, and (f) oil droplet size distribution for all emulsions analyzed using ImageJ software.

pressure to remove the pores so that only the chemistry of the polymer affects the contact angle values. Water has a surface tension of 72.5 mN/m, and diesel has a surface tension of 26 mN/m.

3. RESULTS AND DISCUSSION

3.1. Effect of Polymer Gel Surface Energy on Emulsion Separation. Here, we investigated the oil−water separation performance of four porous polymer gels offering different surface energy values, namely, syndiotactic polystyrene (sPS), polyimide (PI), polyurea (PUA), and silica. The surfactant-stabilized ultralow sulfur diesel (ULSD, oil)-in-water emulsions were used for this purpose. The study examined several questions. First, oil−water emulsions are most stable when surfactant concentrations are above the CMC. Our previous work[24] established strong surfactant adsorption by polymer gels at surfactant concentrations well above the CMC. In this context, can polymer gels break the surfactant-stabilized emulsions by depleting the surfactant molecules from the liquid phase and from the oil−water interfaces? Second, the surfactant adsorption ability of polymer gels is governed by the surface energy values. It was earlier shown that the surfactant adsorption quantity by the polymer gels followed the order sPS > PI > PUA.[24] This result was attributed to high energy interfaces created by the hydrophobic sPS nanofibrils in sPS gels, which led to significant surfactant adsorption. Similar role of surface energy was reported by Vijayendran et al.[49] PI and PUA showed a lower surfactant adsorption performance, as reflected from their lower surface energy compared to sPS. Does this trend extend to surfactant-stabilized oil−water separation?

The high-magnification SEM images and the values of specific surface area, bulk density, and pore sizes of corresponding aerogels are presented in Figure S1 and Table S1. The nanofibrillar polymer network formed by the sPS, PI, and PUA gels with fibril diameter ∼10−30 nm are seen in SEM images (Figure S1). The silica gel formed a pearl-necklace structure by interconnected spherical beads. The specific surface area data are presented in Table S1. It is noted that sPS, PI, PUA, and silica have BET surface areas of 290 ± 20, 614 ± 15, 263 ± 15, and 787 ± 30 m^2/g, respectively. The BET adsorption−desorption isotherms are shown in Figure S2. The silica gel had the greatest mesoporosity ($\phi_{meso} \sim 0.33$) followed by polyimide ($\phi_{meso} \sim 0.11$), polyurea ($\phi_{meso} \sim 0.10$), and sPS ($\phi_{meso} \sim 0.05$). These polymer gels had an open pore network structure that is essential for unrestricted diffusion or movement of the molecules through the gel network. Table 1 lists the interfacial energy values of the four polymer gels obtained from contact angle data of water and diiodomethane on the polymer surfaces. The corresponding interfacial energy values with water are also listed. sPS, a highly hydrophobic polymer, had an interfacial energy of 48.3 mN/m followed by PI, PUA, and silica with interfacial energy values, respectively, 28.7, 13.7, and 3.3 mN/m.

Surfactant molecules occupy liquid−liquid interfaces, such as the unstable oil−water interface, due to their amphiphilic nature. As a high surface area solid polymer gel is brought in contact with an emulsion, the surfactant molecules can distribute themselves between the oil−water interface and the solid polymer gel−water interface as the oil−water−polymer gel system strives to achieve a state of minimum Gibbs free energy.[50] The minimum Gibbs free energy state can be achieved by various means such as via reduction of the number of unstable interfaces in the system,[49] an increase in the favorable interactions, e.g., between the polymer−surfactant molecules promoted via electrostatic forces, hydrogen bonding, hydrophobic interactions, etc., or formation of energetically stable structural organization of the surfactant molecules at polymer surfaces.[37,38,51] In this regard, the first item to consider is the oil−water and polymer−water interfacial energies that would play a significant role in deciding the fate of the surfactant molecules present in the system.

If the oil−water interface had a higher interfacial energy compared to the polymer−water interface, the surfactant

https://doi.org/10.1021/acs.langmuir.4c03496
Langmuir 2024, 40, 24622−24633

would prefer to stay at the oil−water interface, and there would be no demulsification or oil−water separation. On the contrary, if the polymer−water interfacial energy is higher than the oil−water interfacial energy, the surfactants would spontaneously desorb from the oil−water interface and adsorb onto the polymer at the polymer−water interface, leading to lowering of the total energy of the system. This scenario would lead to the demulsification of the oil droplets and their subsequent coalescence and separation from water. The interfacial energy of the oil, in this case, at the ULSD−water interface was measured using the pendant drop method and found to be 21 ± 1 mN/m. The data presented in Table 1 show that two polymer gel systems, namely, sPS and PI, have higher interfacial energy, respectively, 48.3 and 28.7 mN/m than the oil−water interface. The polyurea and silica gels have interfacial energies of 13.7 and 3.3 mN/m, much lower than that of the oil−water system. In view of the above interfacial energy data, the demulsification performance of the polymer gels should follow the order sPS (highest demulsification) > PI > PUA, silica (no demulsification).

The oil−water emulsion separation experiments were performed by bringing different polymer gel specimens into contact with an oil-in-water emulsion stabilized by the Pluronic L35 surfactant for a period of 12 h. The emulsion preparation method was previously presented in the Experimental Section. Optical microscopy images were obtained for the emulsion before and after it was brought in contact with different polymer gels for 12 h. The images are shown in Figure 1a−e. The diameters of a population of about 500 droplets were analyzed for each emulsion to yield a droplet size distribution, as presented in Figure 1f. The control emulsion with droplets shown in Figure 1a and size distribution shown in Figure 1f (light green column) was stable for a week and had a broad oil droplet size distribution ranging from approximately 5−50 μm with a most probable oil droplet size of approximately 20 μm.

The oil−water emulsion specimen exposed to sPS gels showed no visible droplets (Figure 1b). The oil−water emulsion brought in contact with polyimide gels showed visible droplets, as seen in Figure 1c. The oil droplet size distribution shifted significantly toward the left, indicating effective separation of oil droplets of diameters greater than 10 μm. The sPS gel performed the best among the four gels, while the polyimide gel produced moderate separation. This trend is attributed to the higher interfacial energy of the sPS gel compared to the PI gel and, therefore, to greater surfactant adsorption in the case of sPS. The oil−water specimens exposed to polyurea and silica gels showed very little change in the droplet sizes (Figure 1c,d) and their distribution (Figure 1f). Thus, competitive surfactant adsorption on solid gel surfaces governed by corresponding high interfacial energy values is the first evidence that emulsion separation is driven by surfactant adsorption abilities of the polymer gels.

Next is the contribution of oil absorption in the pores of solid gels to oil−water emulsion separation. If it is a case of only surfactant adsorption, the oil droplets would coalesce into bigger droplets accompanied by depletion of the surfactant concentration in the system as shown by several researchers in conjunction with the use of chemical demulsifiers.[3,16,18,23] However, it was not the case as large, coalesced oil droplets were not observed in the emulsion. This brings up the point of volumetric oil absorption by polymer gels.

All polymer gels used in this work had porosity >90% and the open pores were initially filled completely with water. Thus, for oil absorption by the gel, the water present in the pores of the gel must be gradually displaced by the oil. In this context, a simple experiment was performed to illustrate the water displacement ability of the oil phase. Figure 2a,b shows

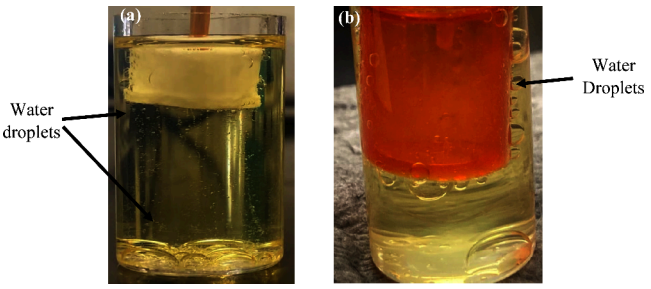

Figure 2. Displacement of water within the pores of the (a) sPS gel and (b) PI gel when it is brought in contact with ULSD (oil).

the snapshots of water-filled sPS and PI gels when brought in contact with ULSD (oil phase). In the case of the sPS gel, an instantaneous displacement of water by the oil phase was observed (Figure 2a). The water from within the gel trickled down as tiny water droplets from the gel surface as the oil phase was absorbed by the gel. This process continued until all water present in the gel was displaced by the oil. A similar phenomenon occurred in the case of the polyimide gel, as seen in Figure 2b, although the rate of water displacement by the oil phase was slow. The water droplets released from the PI gel were found to be much smaller compared to the sPS gel. Also, the water droplets coming out of the PI gel adhered to the gel surface, attributed to the higher polarity of PI compared to the sPS surface (Table 1). Similar experiments with PUA and silica gels showed insignificant oil absorption as reflected from negligible amounts of water released from the gels. We now examine if emulsion separation is governed by surfactant adsorption or merely by oil absorption by the system.

A new set of emulsion separation experiments was performed by bringing the sPS gel in contact with a Pluronic F127 surfactant-stabilized oil-in-water emulsion. An earlier study[24] reported that the sPS gel did not adsorb the Pluronic F127 surfactant as effectively as the Pluronic L35 surfactant. Thus, in the case of Pluronic F127-stabilized emulsion, emulsion separation by the sPS gel should occur primarily by oil absorption. Figure 3 presents several images of droplets taken by using an optical microscope.

A comparison of the images in Figure 3a and Figure 3b reveals a significant reduction of the number of droplets, indicating a certain degree of emulsion separation in contact with the sPS gel. However, in reference to the image presented in Figure 1b, the sPS gel was not as efficient in removal of oil droplets from the F127-stabilized emulsion as it was for the Pluronic L35-stabilized emulsion. This difference can be attributed to the difference in the surfactant adsorption extent of the two surfactants by the sPS gel as the oil absorption capability should be the same in both cases. The larger size Pluronic F127 surfactant molecules did not adsorb onto the sPS gel as much as the smaller molecules of PL35.

We now delve deeper to understand other factors that influence the surfactant adsorption behavior, such as the structural configuration of the adsorbed surfactant molecules, their interaction energy with the solid surface, and their occupied surface area. We resorted to atomistic molecular dynamics simulations to answer these questions.

https://doi.org/10.1021/acs.langmuir.4c03496
Langmuir 2024, 40, 24622−24633

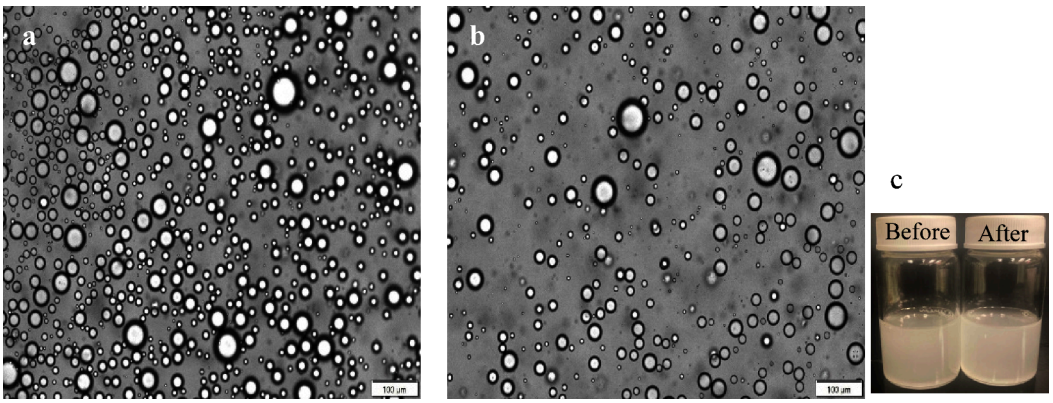

Figure 3. Optical microscopy images for Pluronic F127-stabilized oil-in-water emulsion. (a) Control emulsion (b) in contact with the sPS gel for 12 h and (c) visual images of the emulsion.

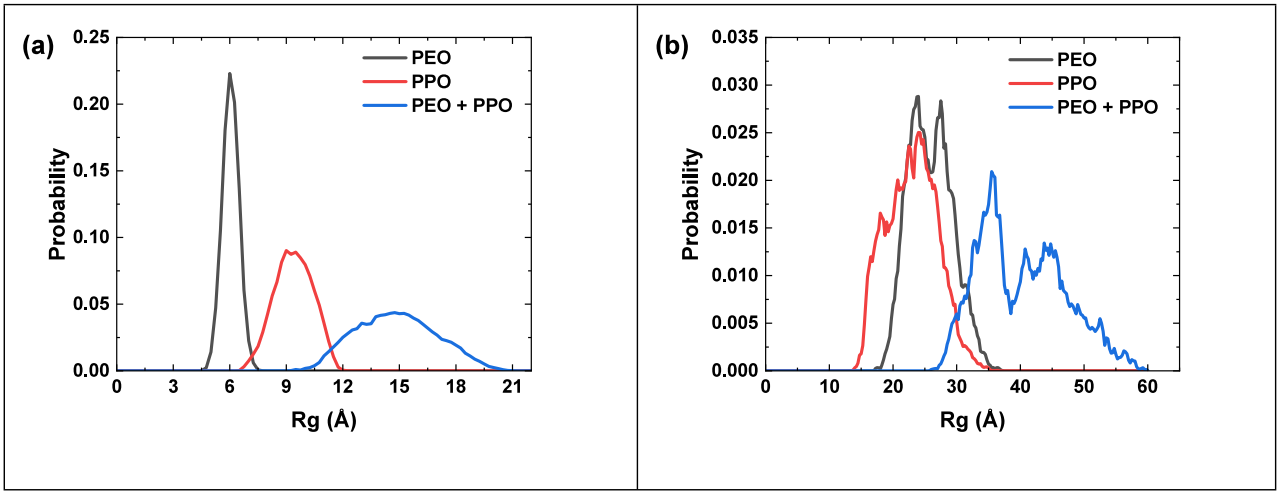

Figure 4. Radius of gyration distribution for the (a) short-chain PL35 surfactant and (b) long-chain PF127 surfactant in water.

3.2. Short-Chain PEO-PPO-PEO Surfactant (PL35) vs Long-Chain PEO-PPO-PEO Surfactant (F127) Adsorption on a Syndiotactic Polystyrene Surface. The extent of surfactant adsorption depends on factors such as the solvent type, adsorbent surface characteristics, types of interactions between the adsorbent−adsorbate or adsorbate−adsorbate, the strength of those interactions, adsorbate size, etc.[50] As these factors work in tandem, it is difficult to identify the primary contributions to the adsorption process. The adsorption isotherms provide valuable information about adsorbed species such as the adsorption energy and probable structural configuration of the adsorbed molecules in the state of equilibrium. In this context, atomistic simulation of the adsorbate−adsorbent system using accurate force fields presents a more reliable approach to obtaining the key dynamic information. Atomistic simulations of the adsorption behavior of PL35 and F127 surfactants in solution on a model sPS surface were conducted. The goal was to understand the difference in adsorption of the two surfactants on the sPS surface, their structural configuration at the surface, their interaction energy, the area occupied by the molecules on the solid surface, and the possibility of aggregation of the surfactant molecules to form higher-order structures on the sPS surface.

First, the behavior of the two surfactant molecules in bulk water was studied. Figure 4 shows the radius of gyration (R_g) distribution for the short-chain (PL35) and long-chain (PF127) surfactant in water where the corresponding R_g values of each PEO and PPO part of the chain as well as the whole single chain are depicted. The time evolution of R_g of L35 and F127 chains in water can be found in Figure S3. The total R_g for L35 was found to oscillate between 1 and 2 nm with an average of 1.47 ± 0.21 nm, while for F127, it oscillated between 2.5 and 6 nm with an average of 4.01 ± 0.68 nm. For L35, the mean R_g values for the PEO and PPO blocks are 0.59 ± 0.06 and 0.92 ± 0.10 nm, respectively. Notably, the PEO block displays a shorter range of oscillations compared to both the PPO block and the entire chain. For the longer PF127 chain, the mean R_g values for the PEO and PPO blocks are 2.56 ± 0.44 and 2.28 ± 0.39 nm, respectively. This is accompanied by a strong oscillation of PEO blocks in contrast to the PPO block. The Gaussian chain characteristics of the PEO and PPO blocks in the chain are evident in both L35 and F127. However, the less smooth curve (with strong fluctuation) observed for F127 indicates a greater need for sampling, requiring significantly longer simulations (>500 ns), which was computationally expensive. Moreover, the findings depicted in Figure S3, which shows the time evolution of R_g, demonstrate the spatial exploration of the chains as they undergo cycles of extension and contraction throughout the simulation process.

https://doi.org/10.1021/acs.langmuir.4c03496
Langmuir 2024, 40, 24622−24633

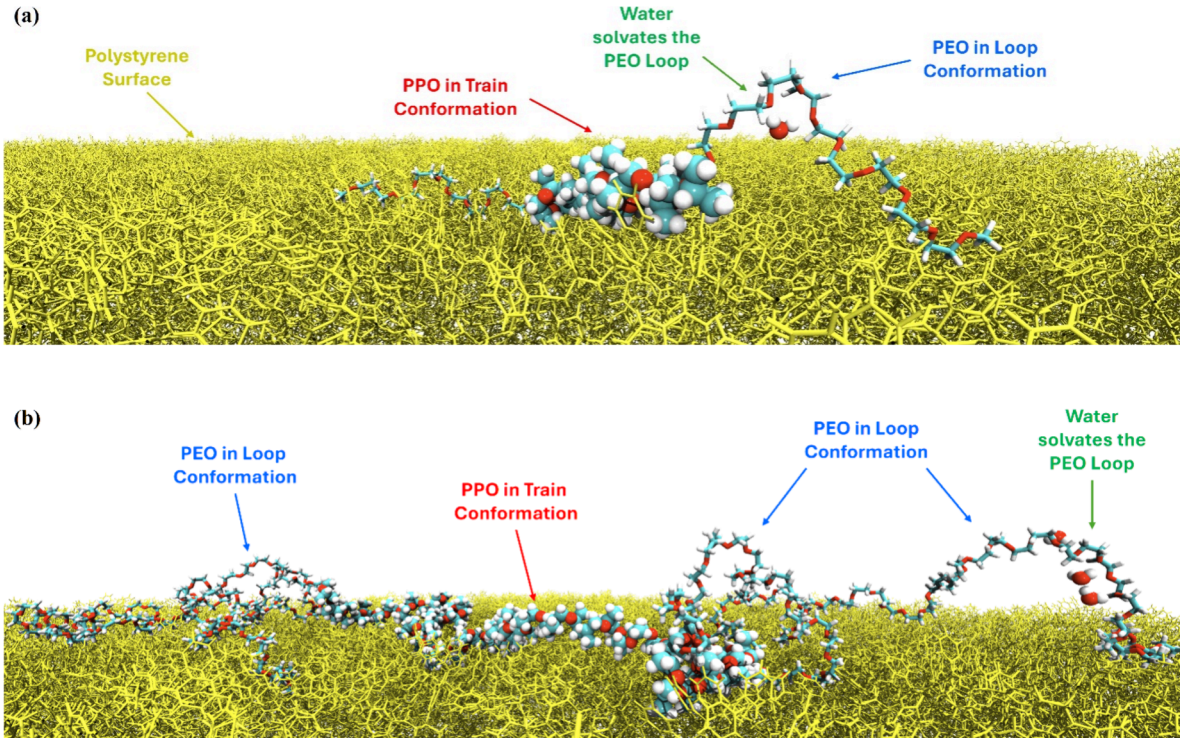

Figure 5. Snapshots of the (a) short-chain PEO-PPO-PEO surfactant (Pluronic L35) and (b) long-chain PEO-PPO-PEO surfactant (Pluronic F127) adsorption on an sPS surface. In the snapshot, the sPS substrate is depicted in yellow, while oxygen, carbon, and hydrogen atoms of the surfactants are colored in red, cyan, and white, respectively. The van der Waals (VdW) representation highlights the PPO block of PL35 and FL127 along with some representative water molecules close to oxygen atoms of the PEO block. The PEO block is illustrated using stick representation.

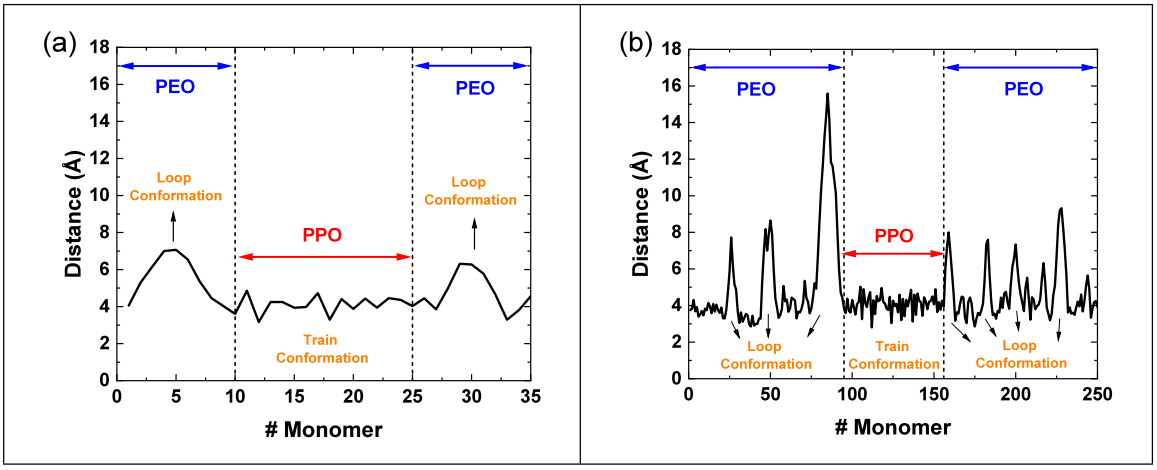

Figure 6. Distance of oxygen in each monomer from the polystyrene surface for the (a) short chain of PL35 and (b) long chain of PF127. The dot lines illustrate the monomer number where the PPO block starts and ends.

Several studies reported adsorption of a PEO-PPO-PEO block copolymer surfactant on solid surfaces.[52] Most of these reported a structural configuration showing PPO segments adsorbing onto the solid surface and the PEO chains remaining extended in the water phase. The pendant methyl group in the PPO chain causes high hydrophobicity and is responsible for the solubility difference between PEO and PPO blocks of the surfactant. In this case, the PPO segment acts as a necessary anchor for the surfactant molecules to adsorb onto the solid surface. The lengths of PPO and PEO segments affect the structural organization of the adsorbed molecules,[48] as it affects the solubility of the molecules in the solvent. Earlier studies reported a phase-separated PPO layer, or formation of loops, train conformations of the PPO segment,[49] or a tightly coiled PPO segment[51] on the solid surfaces. Polystyrene and silica have been frequently studied solid surfaces for adsorption of these molecules. In the case of polystyrene, hydrophobic interactions between the surfactant and surface led to their adsorption, while for the silica surface, hydrogen bonding was found to be the dominant binding mechanism.[34,35,52]

Contrary to literature reports, our simulation results for Pluronic L35 and Pluronic F127 surfactants showed adsorption of both the PEO and PPO segments onto the sPS surface (Figure 5). Figure 6a,b illustrates the distances of each of the monomers of L35 and F127, respectively, with respect to their adjacent sPS surface atoms. Because of the sPS surface

https://doi.org/10.1021/acs.langmuir.4c03496
Langmuir 2024, 40, 24622−24633

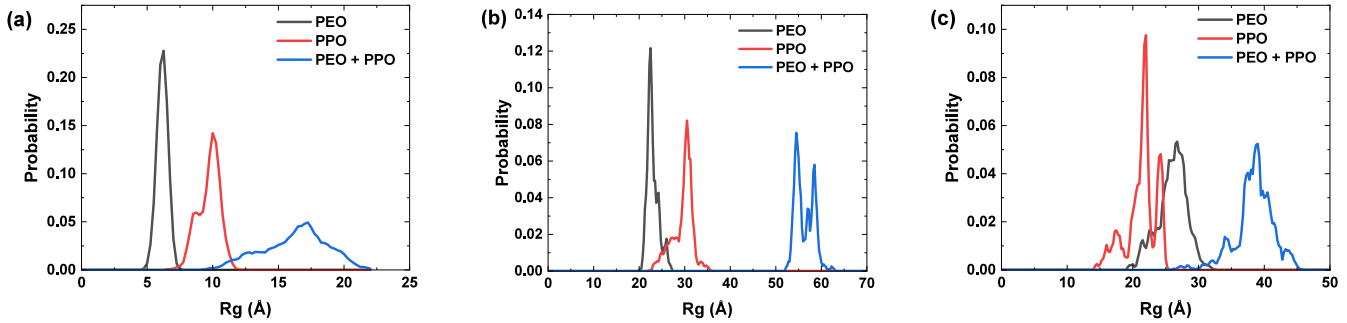

Figure 7. Radius of gyration distribution of the (a) short-single-chain PL35 surfactant, (b) long-chain PF127 surfactant (PEO blocks placed close to the sPS surface), and (c) long-chain PF127 surfactant at the sPS−water interface (PPO blocks placed close to the sPS surface).

roughness, calculating the instantaneous surface was essential, and measuring the monomer distance is required considering the local position of the surface atoms.[53]

In the case of Pluronic L35, the PPO block lies completely flat on the sPS surface in a train conformation, exhibiting strong adsorption of PPO to the surface. Meanwhile, the PEO blocks either adsorb onto the surface or adopt a loop conformation, with the tail conformation being less common. The conformation is different in the case of Pluronic F127, where the PPO block still lies strongly adsorbed onto the sPS surface, and the PEO block adsorbs on the surface partially. The nonadsorbed monomer units form tail and loops on the surface. In other words, the PEO block is adsorbed on the sPS surface only at a certain number of contact points, as shown in Figure 6b. Additionally, the average number of monomers corresponding to loop conformation in L35 (<10) are fewer than those in F127 (>12). This could lead to a more extended loop for F127 as they are farther away from the sPS surface where their interactions with the surface reduced.

Another interesting observation from Figure 5a,b is that the oxygen groups of the PEO and PPO segments usually oriented themselves toward the water phase, thereby maximizing their interactions with the water molecules instead of the sPS surface. This allowed the $-CH_2$ group of the PEO block to interact with the sPS surface and led to its adsorption on the surface. Radius of gyration analysis similar to Figure 4 was made for the case of the surfactants at the sPS−water interface and is shown in Figure 7. For the short Pluronic chain of L35, a single chain was simulated, and the corresponding radius of gyration distribution is shown in Figure 7a. Due to the slower relaxation time of the F127 long chain, two different conformations were prepared to avoid excessive simulation time needed to observe chain adsorption and equilibration. In the first case for F127, the PEO blocks are placed initially in proximity to the sPS surface while the PPO blocks are further away from the surface. The second case was for the conformation where the PPO block is close to the sPS surface, and the PEO tails are placed at further distance relative to the surface. In Figure 7b,c, the radius of gyration distribution as well as their corresponding R_g block are shown for cases one and two, respectively. The adsorption of the surfactant molecule at the sPS−water interface led to restricted movement of the molecule, which is clearly observed by the multiple peaks of the R_g distribution of the molecule. For the short-chain PL35 surfactant depicted in Figure 7a, the molecule seems to lie more in the stretched state with an R_g of 1.61 ± 0.24 nm, whereas in the case of the long-chain PF127 surfactant, the total R_g could be conformation-dependent as multiple adsorption conformation can exist in the experiment, leading to a variability in the measured R_g based on the specific conformational state of the surfactant molecule. For case one, where PEO is initially close to the sPS surface, the R_g value is about 5.70 ± 0.19 nm, which is higher than the corresponding value in the bulk, as shown in Figure 7b. The figure also exhibits that the PPO block is more stretched than the PEO counterparts. However, for the other case, where PPO block is initially placed close to the surface, the average R_g is almost comparable to that of in the bulk, which is about 3.82 ± 0.29 nm, shown in Figure 7c. Unlike case 1, the PPO block has a less degree of extension, where the PEO block has a higher average R_g value. The time evolution radius of gyration for the two surfactants at the sPS−water interface is shown in Figure S4 where the snapshots of corresponding conformation for the minimum and maximum radius of gyration for the short surfactant PL35 are presented in Figure S5. The snapshots illustrate that both PPO and PEO blocks have contributions to the size of the chain while the chain remains adsorbed to the PS interface.

It is known that the oxygen groups on the PEO-PPO-PEO surfactants can form hydrogen bonds with water molecules. The geometrical criteria were employed for hydrogen bond analysis between the oxygen groups of the PEO-PPO-PEO and the hydrogen of the water molecules where further details can be found here.[54] These hydrogen bonding interactions have been quantified in Table 2 for both the short- and long-chain surfactants in bulk water and after their adsorption at the sPS−water interface. For the case of the short-chain PL35 surfactant, the hydrogen bonds per monomer for the PEO blocks did not change (∼1.29) in bulk water and at the sPS−water interface. However, those for the PPO group changed from 1.06 to 0.88 hydrogen bonds per monomer, which

Table 2. Hydrogen Bond per Monomer for the Short- and Long-Chain PEO-PPO-PEO Surfactants in Bulk Water and after Adsorption at the sPS−Water Interface

system		hydrogen bond per monomer
PL35 short chain in water	PEO-	1.29 ± 0.12
	PPO-	1.06 ± 0.08
PL35 short chain at sPS−water interface	PEO-	1.29 ± 0.14
	PPO-	0.88 ± 0.14
PF127 long chain in water	PEO-	1.31 ± 0.04
	PPO-	1.06 ± 0.04
PF127 long chain at sPS−water interface	PEO-	1.21 ± 0.04
	PPO-	0.80 ± 0.05

https://doi.org/10.1021/acs.langmuir.4c03496
Langmuir 2024, 40, 24622−24633

suggests loss of a certain degree of hydrogen bonds by the PPO segment of the surfactant after its adsorption on the sPS surface. For the case of the long-chain PF127 surfactant, the hydrogen bond per monomer for the PEO and PPO groups both reduced from 1.31 (in water) to 1.21 (at the sPS−water interface) and 1.06 (in water) to 0.80 (at the sPS−water interface), respectively. It should be noted that both scenarios (either PEO/PPO initially placed in proximity of sPS) for long-chain F127 lead to the same average values of hydrogen bonds, which shows that hydrogen bonds are local and almost independent of the overall chain conformation. A similar behavior was also observed for a PEO chain at the water/toluene liquid−liquid interface.[55]

To provide additional clarity, we present a comparative analysis of the interaction energies between short-chain and long-chain surfactants with the polymer surface, as shown in Table 3, highlighting the distinct behaviors between these surfactant types. It can be observed that both PEO and PPO segments of the surfactants have favorable interaction energies with the sPS surface, suggested by their large negative values. The interaction energy per PEO monomer was higher for the short-chain surfactant (−2.69 ± 0.77 kcal/mol) compared to the long-chain surfactant (−1.94 ± 0.11 kcal/mol), and this could be because of the formation of loop structures by the PEO block of the long-chain surfactant. The number for case two of PF127 shown in parentheses follows the same trend, while stronger interaction energy exists between PEO and sPS. The interaction energy of the PEO segment per monomer with the surrounding water molecules for the short chain (−16.23 ± 1.65 kcal/mol) was found to be comparable to the long-chain surfactant (−16.39 ± 0.39 kcal/mol). However, the energy fluctuations for the short chain are more than those for long-chain F127. This could result from the lower count of PEO monomers in PL35, making it more reliant on local chain conformations such as loops and tails. The exact reason for the formation of such loop and tail structures by the PEO chain is not exactly known, but it could be to reduce its interaction area with the sPS surface. The PPO segment of the large chain surfactant (−2.83 ± 0.15 kcal/mol) interacts with the sPS surface like the short-chain surfactant (−2.82 ± 0.39 kcal/mol). For case two of the long chain, interaction energy is higher but still looks comparable to the short-chain value once error bars are considered within the calculation. These results raise the question of if both the short-chain and long-chain surfactants show a relatively similar adsorption on the sPS surface with negative interaction energies, why is there disagreement in the simulation results and the experimental adsorption values or their emulsion separation performance?

Table 3. Interaction Energy of the PEO and PPO Segments of the Two Surfactants with the sPS Surface and Water[a]

	Pluronic L35 (short chain)	Pluronic F127 (long chain)
interaction energy per PEO monomer with sPS surface (kcal/mol)	−2.69 ± 0.77	−1.94 ± 0.11 (−2.00 ± 0.10)
interaction energy per PPO monomer with sPS surface (kcal/mol)	−2.82 ± 0.39	−2.83 ± 0.15 (−3.14 ± 0.14)
interaction energy per PEO monomer with water (kcal/mol)	−16.23 ± 1.65	−16.39 ± 0.39 (−16.65 ± 0.40)
interaction energy per PPO monomer with water (kcal/mol)	−11.47 ± 2.03	−10.70 ± 0.47 (−10.42 ± 0.40)

[a]The number in parentheses belongs to case two wherein the initial conformation of the chain the PPO block is placed in proximity to the surface.

There could be several reasons for such observations. Let us look at each of these possible reasons in detail. In an oil-in-water emulsion stabilized by a PEO-PPO-PEO surfactant, the PEO chains remain suspended in the water phase, and the PPO chains interact with the oil phase. Therefore, when an oil droplet stabilized by a surfactant contacts the sPS surface, it is the PEO segment that interacts first with the sPS surface. Therefore, the adsorption effectiveness of the PEO segment would determine the initial threshold to desorb the surfactant from the oil−water interface. In the case of the short-chain surfactant, the PEO segment is short in length with only 10 repeating units, and as shown in Figure 5a, it adsorbs very well on the sPS surface. However, in the case of the Pluronic F127 surfactant, the PEO chain is longer in length with 95 repeating units and does not adsorb as effectively onto the sPS surface, which is evident from the loop structure formation, which suggests that they prefer to stay surrounded by water molecules. Therefore, ineffective adsorption of the PEO segment could be one reason for the difference in the emulsion separation performance. For the Pluronic L35 surfactant, the solvent accessible surface area (SASA) of the molecule on the sPS surface is 2123 Å^2, and similarly, for the

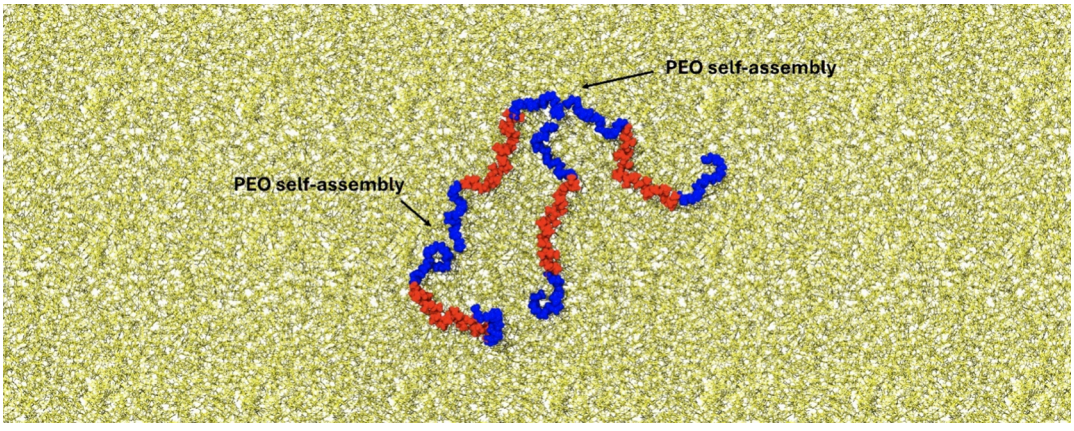

Figure 8. Snapshot of 4 Pluronic L35 surfactant chains adsorbed onto an sPS surface forming a micellar end-to-end connected structure. The PPO and PEO blocks are colored red and blue, respectively.

https://doi.org/10.1021/acs.langmuir.4c03496
Langmuir 2024, 40, 24622−24633

Pluronic F127 surfactant, the SASA value is 14,444 Å^2. Therefore, the higher adsorption surface area required by Pluronic F127 results in limited adsorption of the surfactant from the emulsion and, hence, a comparatively poor emulsion separation performance.

There is another theory explored in this work, which is the structural aggregation of the PEO-PPO-PEO molecules on the sPS surface. Aggregation of surfactants at solid−liquid interfaces has been reported by several researchers.[37,38,56,57] The formation of higher-order structures such as bilayers, hemimicelles, or micelles at the solid−liquid interface has been shown to drive the surfactant adsorption process. A total of four surfactant molecules of the Pluronic L35 surfactant were taken and added to the simulation run along with the sPS surface in the presence of water as the solvent. Given the R_g of the multiple chains shown in Figure S6, the average values are comparable to the single chain. The snapshot of how these four surfactant chains assembled on the sPS surface is shown in Figure 8. It is observed that the Pluronic L35 chains did not adsorb onto the sPS surface at isolated points; rather, they chose to adsorb close to each other, with the PEO-end chains of the surfactant being connected to each other end-to-end and showing the possible micelle formation. To the best of our knowledge, such an end-to-end connected structure formation by a PEO-PPO-PEO block copolymer chain has not been reported in the literature. This type of aggregation suggests a monolayer formation of the block copolymer on the sPS surface. Formation of such a structure on the sPS surface might facilitate the adsorption of a Pluronic L35 surfactant from the liquid phase of the emulsion. A similar calculation could not be performed for the Pluronic F127 case because it is computationally very expensive. However, in the formation of the looping structures by the PEO chains, its attempt to minimize its interaction area with the sPS surface and limited contact points on the sPS surface suggest that there might not be formation of such end-to-end structures in this case. Similarly, simulation studies with adsorption of different surfactants or small molecules such as proteins and PFAS molecules on polymer surfaces would allow a deeper understanding of the effectiveness of their adsorption, the possible structural configurations assumed by these molecules at the interface, their surface coverage, and their interaction energies. These results are anticipated to guide us in screening and developing new materials not only for effective separation of oil−water emulsions but also for separation of small-molecule contaminants from water.

4. CONCLUSIONS

The data in this work suggest that the high surface area meso-macroporous polymer gels are effective media for oil−water emulsion separation. The polymer gels destabilize the emulsion by depleting the surfactant molecules from the liquid system. The emulsion separation ability of the polymer gel scales directly with their surfactant adsorption abilities, and the surfactant adsorption ability in turn has a direct relationship with the surface energy of the polymer gel. The syndiotactic polystyrene gels show a better emulsion separation performance compared with polyimide gels followed by polyurea and silica gel. The removal of the surfactant from the liquid phase triggers absorption of the oil by the porous polymer gel due to preferential wettability for the oil phase. The simulation results show that both the short- and long-chain PEO-PPO-PEO surfactants adsorb on the sPS surface; however, they do so in distinct ways. The short chain lay completely flat on the sPS surface with both the PEO and PPO chains effectively interacting with the sPS surface, whereas for the long-chain surfactant, formation of loop structures by the PEO chains is observed. The area occupied by the short chain on the sPS surface is significantly lower compared to the long-chain surfactant. In addition, the adsorption of four different short-chain molecules on the sPS surface showcases the ability of the surfactant to form higher-order end-to-end connected structures, which might be the reason for its effective adsorption by the sPS gel.

■ ASSOCIATED CONTENT

Data Availability Statement

The raw/processed data required to reproduce these findings cannot be shared at this time as the data also forms part of an ongoing study.

Supporting Information

The Supporting Information is available free of charge at https://pubs.acs.org/doi/10.1021/acs.langmuir.4c03496.

Additional data on SEM morphology, BET, and radius of gyration (PDF)

■ AUTHOR INFORMATION

Corresponding Authors

Mesfin Tsige − *School of Polymer Science and Polymer Engineering, The University of Akron, Akron, Ohio 44325-0301, United States;* orcid.org/0000-0002-7540-2050; Email: mtsige@uakron.edu

Sadhan C. Jana − *School of Polymer Science and Polymer Engineering, The University of Akron, Akron, Ohio 44325-0301, United States;* orcid.org/0000-0001-8962-380X; Email: janas@uakron.edu

Authors

Pratik S. Gotad − *School of Polymer Science and Polymer Engineering, The University of Akron, Akron, Ohio 44325-0301, United States*

Abdol Hadi Mokarizadeh − *School of Polymer Science and Polymer Engineering, The University of Akron, Akron, Ohio 44325-0301, United States;* orcid.org/0000-0001-5922-7654

Complete contact information is available at: https://pubs.acs.org/10.1021/acs.langmuir.4c03496

Author Contributions

[§]P.S.G and A.H.M contributed equally to this work.

Notes

The authors declare no competing financial interest.

■ ACKNOWLEDGMENTS

This work was partially supported by ACS Petroleum Research Fund under grant number PRF# 59000-ND7, U.S. National Science Foundation under grant number CMMI 1826030, DMR-2215940, DMR-2114640, and industrial members of Coalescence Filtration Nanofibers Consortium at The University of Akron

■ REFERENCES

(1) Yonguep, E.; Kapiamba, K. F.; Kabamba, K. J.; Chowdhury, M. Formation, Stabilization and Chemical Demulsification of Crude Oil-

in-Water Emulsions: A Review. *Petroleum Research* **2022**, *7* (4), 459−472.
(2) Liang, H.; Esmaeili, H. Application of Nanomaterials for Demulsification of Oily Wastewater: A Review Study. *Environmental Technology & Innovation* **2021**, *22*, No. 101498.
(3) Wang, D.; Yang, D.; Huang, C.; Huang, Y.; Yang, D.; Zhang, H.; Liu, Q.; Tang, T.; Gamal El-Din, M.; Kemppi, T.; Perdicakis, B.; Zeng, H. Stabilization Mechanism and Chemical Demulsification of Water-in-Oil and Oil-in-Water Emulsions in Petroleum Industry: A Review. *Fuel* **2021**, *286*, No. 119390.
(4) Shehzad, F.; Hussein, I. A.; Kamal, M. S.; Ahmad, W.; Sultan, A. S.; Nasser, M. S. Polymeric Surfactants and Emerging Alternatives Used in the Demulsification of Produced Water: A Review. *Polym. Rev.* **2018**, *58* (1), 63−101.
(5) Martínez-Palou, R.; Cerón-Camacho, R.; Chávez, B.; Vallejo, A. A.; Villanueva-Negrete, D.; Castellanos, J.; Karamath, J.; Reyes, J.; Aburto, J. Demulsification of Heavy Crude Oil-in-Water Emulsions: A Comparative Study between Microwave and Thermal Heating. *Fuel* **2013**, *113*, 407−414.
(6) Xia, L.; Lu, S.; Cao, G. Stability and Demulsification of Emulsions Stabilized by Asphaltenes or Resins. *J. Colloid Interface Sci.* **2004**, *271* (2), 504−506.
(7) Binner, E. R.; Robinson, J. P.; Silvester, S. A.; Kingman, S. W.; Lester, E. H. Investigation into the Mechanisms by Which Microwave Heating Enhances Separation of Water-in-Oil Emulsions. *Fuel* **2014**, *116*, 516−521.
(8) Kocherginsky, N. M.; Tan, C. L.; Lu, W. F. Demulsification of Water-in-Oil Emulsions via Filtration through a Hydrophilic Polymer Membrane. *J. Membr. Sci.* **2003**, *220* (1), 117−128.
(9) Hu, J.; Chen, J.; Zhang, X.; Xiao, J.; An, S.; Luan, Z.; Liu, F.; Zhang, B. Dynamic Demulsification of Oil-in-Water Emulsions with Electrocoalescence: Diameter Distribution of Oil Droplets. *Sep. Purif. Technol.* **2021**, *254*, No. 117631.
(10) Luo, X.; Gong, H.; Yin, H.; He, Z.; He, L. Optimization of Acoustic Parameters for Ultrasonic Separation of Emulsions with Different Physical Properties. *Ultrasonics Sonochemistry* **2020**, *68*, No. 105221.
(11) Chen, X.; Chen, D.; Li, N.; Xu, Q.; Li, H.; He, J.; Lu, J. Durable and Stable MnMoO4-Coated Copper Mesh for Highly Efficient Oil-in-Water Emulsion Separation and Photodegradation of Organic Contaminants. *ACS Appl. Mater. Interfaces* **2019**, *9*, 23789.
(12) Kong, J.; Li, K. Oil Removal from Oil-in-Water Emulsions Using PVDF Membranes. *Sep. Purif. Technol.* **1999**, *16* (1), 83−93.
(13) Gotad, P. S.; Kafle, N.; Miyoshi, T.; Jana, S. C. Meso- and Macroporous Polymer Gels for Efficient Adsorption of Block Copolymer Surfactants. *Langmuir* **2022**, *38* (44), 13558−13568.
(14) Gotad, P. S.; Jana, S. C. Aerogel-Glass Fiber Composite Filter Media for Effective Separation of Emulsified Water Droplets from Diesel Fuel. *Sep. Purif. Technol.* **2024**, *332*, No. 125705.
(15) Kilpatrick, P. K. Water-in-Crude Oil Emulsion Stabilization: Review and Unanswered Questions. *Energy Fuels* **2012**, *26* (7), 4017−4026.
(16) Katepalli, H.; Bose, A.; Hatton, T. A.; Blankschtein, D. Destabilization of Oil-in-Water Emulsions Stabilized by Non-Ionic Surfactants: Effect of Particle Hydrophilicity. *Langmuir* **2016**, *32* (41), 10694−10698.
(17) Le Follotec, A.; Pezron, I.; Noik, C.; Dalmazzone, C.; Metlas-Komunjer, L. Triblock Copolymers as Destabilizers of Water-in-Crude Oil Emulsions. *Colloids Surf., A* **2010**, *365* (1), 162−170.
(18) Liu, J.; Li, X.; Jia, W.; Li, Z.; Zhao, Y.; Ren, S. Demulsification of Crude Oil-in-Water Emulsions Driven by Graphene Oxide Nanosheets. *Energy Fuels* **2015**, *29* (7), 4644−4653.
(19) Sun, H.; Wang, Q.; Li, X.; He, X. Novel Polyether-Polyquaternium Copolymer as an Effective Reverse Demulsifier for O/W Emulsions: Demulsification Performance and Mechanism. *Fuel* **2020**, *263*, No. 116770.
(20) *Synthesis of a novel copolymer of block polyether macromonomer and diallyldimethylammonium chloride and its reverse demulsification performance* | Elsevier Enhanced Reader. .
(21) Hao, L.; Jiang, B.; Zhang, L.; Yang, H.; Sun, Y.; Wang, B.; Yang, N. Efficient Demulsification of Diesel-in-Water Emulsions by Different Structural Dendrimer-Based Demulsifiers. *Ind. Eng. Chem. Res.* **2016**, *55* (6), 1748−1759.
(22) Lemos, R. C. B.; da Silva, E. B.; dos Santos, A.; Guimarães, R. C. L.; Ferreira, B. M. S.; Guarnieri, R. A.; Dariva, C.; Franceschi, E.; Santos, A. F.; Fortuny, M. Demulsification of Water-in-Crude Oil Emulsions Using Ionic Liquids and Microwave Irradiation. *Energy Fuels* **2010**, *24* (8), 4439−4444.
(23) Silva, E. B.; Santos, D.; Alves, D. R. M.; Barbosa, M. S.; Guimarães, R. C. L.; Ferreira, B. M. S.; Guarnieri, R. A.; Franceschi, E.; Dariva, C.; Santos, A. F.; Fortuny, M. Demulsification of Heavy Crude Oil Emulsions Using Ionic Liquids. *Energy Fuels* **2013**, *27* (10), 6311−6315.
(24) Shinko, A.; Jana, S. C.; Meador, M. A. Crosslinked Polyurea Aerogels with Controlled Porosity. *RSC Adv.* **2015**, *5* (127), 105329−105338.
(25) Daniel, C.; Dammer, C.; Guenet, J.-M. On the Definition of Thermoreversible Gels: The Case of Syndiotactic Polystyrene. *Polymer* **1994**, *35* (19), 4243−4246.
(26) Meador, M. A. B.; Malow, E. J.; Silva, R.; Wright, S.; Quade, D.; Vivod, S. L.; Guo, H.; Guo, J.; Cakmak, M. Mechanically Strong, Flexible Polyimide Aerogels Cross-Linked with Aromatic Triamine. *ACS Appl. Mater. Interfaces* **2012**, *4* (2), 536−544.
(27) Kulkarni, A.; Gotad, P.; Joo, P.; Agrawal, A.; Chase, G. C.; Jana, S. C. Water Separation from Diesel Fuel Using High Surface Area 3D-Printed Aerogel Constructs. *Sep. Purif. Technol.* **2024**, *328*, No. 125065.
(28) Daniel, C.; Menelle, A.; Brulet, A.; Guenet, J. m. Thermoreversible Gelation of Syndiotactic Polystyrene: Effect of Solvent Type. *Macromol. Symp.* **1997**, *114* (1), 159−164.
(29) Krishnan, V. G.; Joseph, A. M.; Kuzhichalil Peethambharan, S.; Gowd, E. B. Nanoporous Crystalline Aerogels of Syndiotactic Polystyrene: Polymorphism, Dielectric, Thermal, and Acoustic Properties. *Macromolecules* **2021**, *54* (22), 10605−10615.
(30) Guo, H.; Meador, M. A. B.; McCorkle, L.; Quade, D. J.; Guo, J.; Hamilton, B.; Cakmak, M.; Sprowl, G. Polyimide Aerogels Cross-Linked through Amine Functionalized Polyoligomeric Silsesquioxane. *ACS Appl. Mater. Interfaces* **2011**, *3* (2), 546−552.
(31) Teo, N.; Jana, S. C. Solvent Effects on Tuning Pore Structures in Polyimide Aerogels. *Langmuir* **2018**, *34* (29), 8581−8590.
(32) *Multifunctional Polyurea Aerogels from Isocyanates and Water. A Structure−Property Case Study* | Chemistry of Materials. https://pubs.acs.org/doi/10.1021/cm102891d.
(33) Mawhinney, K.; Jana, S. C. Design Of Emulsion-Templated Mesoporous−Macroporous Polyurea Gels and Aerogels. *ACS Appl. Polym. Mater.* **2019**, *1* (11), 3115−3129.
(34) Long, L.-Y.; Weng, Y.-X.; Wang, Y.-Z. Cellulose Aerogels: Synthesis, Applications, and Prospects. *Polymers* **2018**, *10* (6), 623.
(35) Hüsing, N.; Schubert, U. Organofunctional Silica Aerogels. *J. Sol-Gel Sci. Technol.* **1997**, *8* (1), 807−812.
(36) Biesmans, G.; Randall, D.; Francais, E.; Perrut, M. Polyurethane-Based Organic Aerogels' Thermal Performance. *J. Non-Cryst. Solids* **1998**, *225*, 36−40.
(37) Shin, T. G.; Müter, D.; Meissner, J.; Paris, O.; Findenegg, G. H. Structural Characterization of Surfactant Aggregates Adsorbed in Cylindrical Silica Nanopores. *Langmuir* **2011**, *27* (9), 5252−5263.
(38) Tiberg, F. Physical Characterization of Non-Ionic Surfactant Layers Adsorbed at Hydrophilic and Hydrophobic Solid Surfaces by Time-Resolved Ellipsometry. *Faraday Trans.* **1996**, *92* (4), 531.
(39) Paria, S.; Manohar, C.; Khilar, K. C. Adsorption of Anionic and Non-Ionic Surfactants on a Cellulosic Surface. *Colloids Surf., A* **2005**, *252* (2−3), 221−229.
(40) Abbott, L. J.; Hart, K. E.; Colina, C. M. Polymatic: A Generalized Simulated Polymerization Algorithm for Amorphous Polymers. *Theor. Chem. Acc.* **2013**, *132* (3), 1334.
(41) Thompson, A. P.; Aktulga, H. M.; Berger, R.; Bolintineanu, D. S.; Brown, W. M.; Crozier, P. S.; in 't Veld, P. J.; Kohlmeyer, A.; Moore, S. G.; Nguyen, T. D.; Shan, R.; Stevens, M. J.; Tranchida, J.;

https://doi.org/10.1021/acs.langmuir.4c03496
Langmuir 2024, 40, 24622−24633

Trott, C.; Plimpton, S. J. LAMMPS - a Flexible Simulation Tool for Particle-Based Materials Modeling at the Atomic, Meso, and Continuum Scales. *Comput. Phys. Commun.* **2022**, *271*, No. 108171.
(42) Berendsen, H. J. C.; Grigera, J. R.; Straatsma, T. P. The Missing Term in Effective Pair Potentials. *J. Phys. Chem.* **1987**, *91* (24), 6269−6271.
(43) Ileri Ercan, N.; Stroeve, P.; Tringe, J. W.; Faller, R. Understanding the Interaction of Pluronics L61 and L64 with a DOPC Lipid Bilayer: An Atomistic Molecular Dynamics Study. *Langmuir* **2016**, *32* (39), 10026−10033.
(44) Hockney, R. W.; Eastwood, J. W. *Computer Simulation Using Particles*; CRC Press: Boca Raton, 2021. .
(45) Ryckaert, J.-P.; Ciccotti, G.; Berendsen, H. J. C. Numerical Integration of the Cartesian Equations of Motion of a System with Constraints: Molecular Dynamics of *n*-Alkanes. *J. Comput. Phys.* **1977**, *23* (3), 327−341.
(46) Bekele, S.; Tsige, M. Interfacial Properties of Oxidized Polystyrene and Its Interaction with Water. *Langmuir* **2013**, *29* (43), 13230−13238.
(47) Watkins, E. K.; Jorgensen, W. L. Perfluoroalkanes: Conformational Analysis and Liquid-State Properties from Ab Initio and Monte Carlo Calculations. *J. Phys. Chem. A* **2001**, *105* (16), 4118−4125.
(48) Wu, S. Calculation of Interfacial Tension in Polymer Systems. *Journal of Polymer Science Part C: Polymer Symposia* **1971**, *34* (1), 19−30.
(49) Vijayendran, B. R. Polymer Polarity and Surfactant Adsorption. *J. Appl. Polym. Sci.* **1979**, *23* (3), 733−742.
(50) Somasundaran, P.; Shrotri, S.; Huang, L. Thermodynamics of Adsorption of Surfactants at Solid-Liquid Interface. *Pure Appl. Chem.* **1998**, *70* (3), 621−626.
(51) Zhu, B.-Y.; Gu, T. Surfactant Adsorption at Solid-Liquid Interfaces. *Adv. Colloid Interface Sci.* **1991**, *37* (1), 1−32.
(52) Alexandridis, P.; Alan Hatton, T. Poly(Ethylene Oxide)—poly(Propylene Oxide)—poly(Ethylene Oxide) Block Copolymer Surfactants in Aqueous Solutions and at Interfaces: Thermodynamics, Structure, Dynamics, and Modeling. *Colloids Surf., A* **1995**, *96* (1), 1−46.
(53) Baker, J. A.; Berg, J. C. Investigation of the Adsorption Configuration of Polyethylene Oxide and Its Copolymers with Polypropylene Oxide on Model Polystyrene Latex Dispersions. *Langmuir* **1988**, *4* (4), 1055−1061.
(54) Bekele, S.; Tsige, M. Effect of Polymer/Solid and Polymer/Vapor Instantaneous Interfaces on the Interfacial Structure and Dynamics of Polymer Melt Systems. *Langmuir* **2016**, *32* (28), 7151−7158.
(55) Shandiz, S. A.; Leuty, G. M.; Guo, H.; Mokarizadeh, A. H.; Maia, J. M.; Tsige, M. Structure and Thermodynamics of Linear, Ring, and Catenane Polymers in Solutions and at Liquid−Liquid Interfaces. *Langmuir* **2023**, *39* (20), 7154−7166.
(56) Domínguez, H. Self-Aggregation of the SDS Surfactant at a Solid−Liquid Interface. *J. Phys. Chem. B* **2007**, *111* (16), 4054−4059.
(57) Király, Z.; Börner, R. H. K.; Findenegg, G. H. Adsorption and Aggregation of C8E4 and C8G1 Nonionic Surfactants on Hydrophilic Silica Studied by Calorimetry. *Langmuir* **1997**, *13* (13), 3308−3315.

https://doi.org/10.1021/acs.langmuir.4c03496
Langmuir 2024, 40, 24622−24633